Bayesian Techniques for Edge Detection on Polarimetric SAR Images

Francesco Bandiera, Antonio Masciullo, and Giuseppe Ricci
University of Salento, Dipartimento di Ingegneria dell'Innovazione
Via Monteroni, 73100 Lecce (LE), Italy
E-Mail: name.surname@unisalento.it

***Abstract*—We propose a Bayesian edge detector to be fed by polarimetric, possibly multifrequency, SAR data. It can be used to detect dark spots on the ocean surface and, hence, as the first stage of a system for identification and monitoring of oil spills. The proposed detector does not require secondary data (namely pixels from a slick-free area), but for a certain a priori knowledge about the spectral properties of the data. The performance assessment, carried out using both synthetic and real SAR recordings, shows that it has better capabilities in terms of detection and false alarms control than previously-proposed classical (i.e., non-Bayesian) detectors.**

I. Introduction

Synthetic Aperture Radars (SARs) represent a powerful tool for monitoring oil spills on the sea surface. In practice, oil floating on the sea surface reduces the energy backscattered by the illuminated area since oil slicks produce an increased viscosity of the top layer of the sea surface which damps out the short gravity and capillary waves responsible for the amount of backscattered energy measured by the SAR [1]. Nevertheless, other phenomena can produce the same effect on SAR images (the so-called look-alikes), as low wind, grease ice, internal waves, rain cells, and biogenic films. For this reason, monitoring oil spills on the sea surface is a very challenging task and requires advanced functionalities in order to discriminate between real oil spills and look-alikes [2]-[5]. In order to increase the detectability of slicks, it has been proposed to use both multifrequency and multipolarization data [6]-[14]. In many cases, proposed algorithms assume that a set of secondary data, i.e., a slick-free area, is available. However, the availability of such data might be difficult to meet in many situations of practical interest. In [8]-[12] edge detectors (EDs) based upon the generalized likelihood ratio test (GLRT) to be fed by polarimetric and/or multifrequency data have been proposed. The design of the GLRTs relies on the assumption that pixels of either a slick-free or a slick-covered area, within the region under test, can be modeled in terms of Gaussian vectors with a common (unknown) covariance matrix. Remarkably, such schemes guarantee the constant false alarm rate (CFAR) property and, above all, have been proven effective on real data recordings.

In this paper, we extend the idea to a Bayesian framework. The Bayesian approach has been already used in the field of adaptive radar detection in non-homogeneous environments, see, e.g., [15], [16]. In fact, Bayesian tools are effective to handle heterogeneities and to include a priori information. The idea herein pursued is to assume that the covariance matrix of each pixel is a random quantity with some preassigned a priori distribution. The adaptive detector can be obtained averaging out the random covariance matrices from the likelihood functions.

The remaining of the paper is organized as follows: Section II is devoted to the problem formulation and to the design of the edge detector while in Section III we carry out a performance assessment based upon both simulated and real SAR data.

II. Problem Formulation and Detector Design

Denote by $\boldsymbol{r}_{i,j}$ the N-dimensional vector whose n-th entry, $r_{i,j}(n)$ say, is the complex reflectivity of the (i,j)-th pixel of the SAR image in the n-th polarimetric channel, $n=1,\ldots,N$, i.e., $\boldsymbol{r}_{i,j} = [r_{i,j}(1)\cdots r_{i,j}(N)]^T$ where ^{T} denotes transpose. The aim is to conceive a detector to discriminate between the H_0 hypothesis that M adjacent pixels belong to either a slick-free or a slick-covered area and the alternative H_1 that they contain the edge of a slick. To this end, denote by $\mathcal{S}$ the set of all pairs of indices corresponding to the M pixels under test; the idea is that, if those M adjacent pixels contain the edge, the slick does not cover the entire region under test and we can split returns into two groups according to their statistical characterization. Consequently, from a statistical point of view, we suppose that, conditionally to the covariance matrix, $\boldsymbol{R}_{i,j}$ say, polarimetric return $\boldsymbol{r}_{i,j}$ is a zero-mean, complex normal random vector [17]; in addition, conditionally to the $\boldsymbol{R}_{i,j}$s, the $\boldsymbol{r}_{i,j}$s are independent random vectors. In symbols, we write $\boldsymbol{r}_{i,j}|\boldsymbol{R}_{i,j} \sim \mathcal{CN}_N(\boldsymbol{0}, \boldsymbol{R}_{i,j})$. Moreover, we assume that $\boldsymbol{R}_{i,j}$ is drawn from a complex inverse Wishart distribution, with *known* mean $\overline{\boldsymbol{R}}$ and ν ($> N$) degrees of freedom; the corresponding probability density function (pdf) can be written as

$$p(\boldsymbol{R}_{i,j}) = \frac{\left|(\nu-N)\overline{\boldsymbol{R}}\right|^{\nu}}{\widetilde{\Gamma}_N(\nu)\left|\boldsymbol{R}_{i,j}\right|^{\nu+N}} \mathrm{etr}\left\{-(\nu-N)\boldsymbol{R}_{i,j}^{-1}\overline{\boldsymbol{R}}\right\} \qquad (1)$$

where $|\cdot|$ is the determinant of the matrix argument, $\mathrm{etr}(\cdot)$ stands for the exponential of the trace of the matrix argument, and $\widetilde{\Gamma}_N(\nu)$ is given by

$$\widetilde{\Gamma}_N(\nu) = \pi^{\frac{N(N-1)}{2}} \prod_{n=1}^{N} \Gamma(\nu-n+1)$$

with $\Gamma(x)$ being, in turn, the Eulerian Gamma function. We denote this distribution as $\boldsymbol{R}_{i,j} \sim \mathcal{CW}^{-1}\left((\nu-N)\overline{\boldsymbol{R}}, \nu\right)$. It is worth highlighting the role of the parameters of the distribution. In fact, $\overline{\boldsymbol{R}}$ represents the expected value of $\boldsymbol{R}_{i,j}$ while ν sets the "distance" between $\overline{\boldsymbol{R}}$ and $\boldsymbol{R}_{i,j}$; as ν increases

978-1-4673-3146-3/13/$31.00 ©2013IEEE

$\boldsymbol{R}_{i,j}$ is closer to $\overline{\boldsymbol{R}}$ (in the sense that the variance of $\boldsymbol{R}_{i,j}$ decreases). Such a model allows to take into account a certain statistical variability of polarimetric returns on a pixel-by-pixel basis. In fact, we could even suppose that the $\boldsymbol{R}_{i,j}$s are independent random matrices. However, for the case at hand, it is reasonable to assume that pixels in spatial proximity of either a slick-free or a slick-covered area possess one and the same value of the covariance matrix. In other words, we assume that $\boldsymbol{R}_{i,j} = \boldsymbol{M}_1$ for pixels that belong to the slick and $\boldsymbol{R}_{i,j} = \boldsymbol{M}_0$ for the remaining pixels of the slick-free area. Accordingly, we set $\boldsymbol{M}_1 \sim \mathcal{CW}^{-1}\left((\nu_1 - N)\overline{\boldsymbol{M}}_1, \nu_1\right)$, $\boldsymbol{M}_0 \sim \mathcal{CW}^{-1}\left((\nu_0 - N)\overline{\boldsymbol{M}}_0, \nu_0\right)$, and suppose that $\boldsymbol{M}_1$ and $\boldsymbol{M}_0$ are independent random matrices. $\overline{\boldsymbol{M}}_0$, ν_0, $\overline{\boldsymbol{M}}_1$, and ν_1 represent the a priori knowledge on the problem at hand. In Section III we discuss how to set them. It follows that the detection problem to be solved can be restated in terms of the following binary hypothesis test

$$\begin{cases} H_0 : \begin{cases} \boldsymbol{r}_{i,j}|\boldsymbol{M}_h \sim \mathcal{CN}_N\left(\boldsymbol{0}, \boldsymbol{M}_h\right), & (i,j) \in \mathcal{S} \\ \boldsymbol{M}_h \sim \mathcal{CW}^{-1}\left((\nu_h - N)\overline{\boldsymbol{M}}_h, \nu_h\right), & h = 0 \text{ or } 1 \end{cases} \\ H_1 : \begin{cases} \boldsymbol{r}_{i,j}|\boldsymbol{M}_1 \sim \mathcal{CN}_N\left(\boldsymbol{0}, \boldsymbol{M}_1\right), & (i,j) \in \mathcal{S}_1 \\ \boldsymbol{M}_1 \sim \mathcal{CW}^{-1}\left((\nu_1 - N)\overline{\boldsymbol{M}}_1, \nu_1\right), \\ \boldsymbol{r}_{i,j}|\boldsymbol{M}_0 \sim \mathcal{CN}_N\left(\boldsymbol{0}, \boldsymbol{M}_0\right), & (i,j) \in \mathcal{S}_0 \\ \boldsymbol{M}_0 \sim \mathcal{CW}^{-1}\left((\nu_0 - N)\overline{\boldsymbol{M}}_0, \nu_0\right), \end{cases} \end{cases} \tag{2}$$

where $h = 1$ ($h = 0$) if the region under test is completely covered by the slick (the sea), while the pair $(\mathcal{S}_0, \mathcal{S}_1)$ is an unknown partition of the set $\mathcal{S}$, denoted in the following as $\mathcal{P}_{\mathcal{S}}$; in particular, $\mathcal{S}_1$ is a proper subset of $\mathcal{S}$ and represents the region covered by the slick (under H_1), while $\mathcal{S}_0$ is the complement of $\mathcal{S}_1$ with respect to $\mathcal{S}$. For future convenience, let us denote by M_0 and M_1 the cardinalities of $\mathcal{S}_0$ and $\mathcal{S}_1$, respectively (it is then apparent that $M = M_0 + M_1$, $M_1 \neq M$). Thus, h, under H_0, and the pair $(\mathcal{S}_0, \mathcal{S}_1)$, under H_1, are unknown quantities. Summarizing, we are modeling the pixels of the region under test in terms of the conditionally, given the covariance matrices, complex normal model and testing whether the region can be partitioned into two (unknown) subsets corresponding to two (random) covariance matrices (for slick-free and slick-covered areas), as an alternative to the same (random) covariance matrix. According to the Neyman-Pearson criterion, the optimum solution to the hypotheses testing problem (2) is the likelihood ratio test, but, for the case at hand, it cannot be implemented since total ignorance of the parameter h, under H_0, and the pair $(\mathcal{S}_0, \mathcal{S}_1)$, under H_1, is assumed. We thus switch to a GLRT-based decision scheme. The GLRT is tantamount to replace the unknown parameters with their maximum likelihood estimates under each hypothesis based on the entirety of data, namely to implement the following decision rule

$$\Lambda(\boldsymbol{r}) = \frac{\max\limits_{\mathcal{P}_{\mathcal{S}} \in \mathcal{G}(\mathcal{S})} p(\boldsymbol{r}|\mathcal{P}_{\mathcal{S}}, H_1)}{\max\limits_{h \in \{0,1\}} p(\boldsymbol{r}|h, H_0)} \underset{H_0}{\overset{H_1}{\gtrless}} \gamma \tag{3}$$

where $\boldsymbol{r}$ denotes the vector obtained by stacking up the vectors $\boldsymbol{r}_{i,j}$, $(i,j) \in \mathcal{S}$, $\mathcal{G}(\mathcal{S})$ is a collection of partitions of $\mathcal{S}$, $p(\boldsymbol{r}|\mathcal{P}_{\mathcal{S}}, H_1)$ and $p(\boldsymbol{r}|h, H_0)$ are pdfs of $\boldsymbol{r}$ under H_1 and H_0, respectively, and γ is the threshold value set in order to ensure the desired probability of false alarm (P_{fa}). Subsequent developments require specifying the pdf of $\boldsymbol{r}$ under both hypotheses. Previous assumptions imply that the pdf of $\boldsymbol{r}$, given $\boldsymbol{M}_h$ under H_0 and given $\boldsymbol{M}_0$ and $\boldsymbol{M}_1$ under H_1, can be written as

$$p(\boldsymbol{r}|\boldsymbol{M}_h, H_0) = \left[\frac{1}{\pi^N |\boldsymbol{M}_h|}\right]^M \text{etr}\left[-\boldsymbol{M}_h^{-1} \sum_{(i,j)\in\mathcal{S}} \boldsymbol{r}_{i,j}\boldsymbol{r}_{i,j}^{\dagger}\right]$$

under the H_0 hypothesis and

$$\begin{aligned} p(\boldsymbol{r}|\mathcal{P}_{\mathcal{S}}, &\boldsymbol{M}_0, \boldsymbol{M}_1, H_1) \\ &= \left(\frac{1}{\pi^N |\boldsymbol{M}_0|}\right)^{M_0} \text{etr}\left[-\boldsymbol{M}_0^{-1} \sum_{(i,j)\in\mathcal{S}_0} \boldsymbol{r}_{i,j}\boldsymbol{r}_{i,j}^{\dagger}\right] \\ &\times \left(\frac{1}{\pi^N |\boldsymbol{M}_1|}\right)^{M_1} \text{etr}\left[-\boldsymbol{M}_1^{-1} \sum_{(i,j)\in\mathcal{S}_1} \boldsymbol{r}_{i,j}\boldsymbol{r}_{i,j}^{\dagger}\right] \end{aligned}$$

under the H_1 hypothesis, where † denotes conjugate transpose. Moreover, the pdf of $\boldsymbol{r}$, under H_0, can be computed averaging $\boldsymbol{M}_h$ out of the $p(\boldsymbol{r}|\cdot)$

$$p(\boldsymbol{r}|h, H_0) = \int p(\boldsymbol{r}|\boldsymbol{M}_h, H_0) p(\boldsymbol{M}_h) d\boldsymbol{M}_h.$$

Similarly, we have that

$$\begin{aligned} p(\boldsymbol{r}|\mathcal{P}_{\mathcal{S}}, H_1) = \int &p(\boldsymbol{r}|\mathcal{P}_{\mathcal{S}}, \boldsymbol{M}_0, \boldsymbol{M}_1, H_1) \\ &\times p(\boldsymbol{M}_1) p(\boldsymbol{M}_0) d\boldsymbol{M}_1 d\boldsymbol{M}_0. \end{aligned}$$

Using the fact that the inverse Wishart distribution is a conjugate prior [18], the above integrals can be easily computed (see also [15]) and, after some algebra, the GLRT can be re-written (up to an irrelevant positive factor) as

$$\begin{aligned} &\min_{h\in\{0,1\}} \frac{\widetilde{\Gamma}_N(\nu_h)\left|\sum_{(i,j)\in\mathcal{S}} \boldsymbol{r}_{i,j}\boldsymbol{r}_{i,j}^{\dagger} + (\nu_h - N)\overline{\boldsymbol{M}}_h\right|^{\nu_h + M}}{\widetilde{\Gamma}_N(\nu_h + M)\left|(\nu_h - N)\overline{\boldsymbol{M}}_h\right|^{\nu_h}} \\ &\times \max_{\mathcal{P}_{\mathcal{S}}\in\mathcal{G}(\mathcal{S})} \left\{ \frac{\widetilde{\Gamma}_N(\nu_0 + M_0)}{\left|\sum_{(i,j)\in\mathcal{S}_0} \boldsymbol{r}_{i,j}\boldsymbol{r}_{i,j}^{\dagger} + (\nu_0 - N)\overline{\boldsymbol{M}}_0\right|^{\nu_0 + M_0}} \right. \\ &\left. \times \frac{\widetilde{\Gamma}_N(\nu_1 + M_1)}{\left|\sum_{(i,j)\in\mathcal{S}_1} \boldsymbol{r}_{i,j}\boldsymbol{r}_{i,j}^{\dagger} + (\nu_1 - N)\overline{\boldsymbol{M}}_1\right|^{\nu_1 + M_1}} \right\} \underset{H_0}{\overset{H_1}{\lessgtr}} \gamma. \end{aligned} \tag{4}$$

Now it only remains to perform maximization with respect to the unknown partition $\mathcal{P}_{\mathcal{S}}$ of the set $\mathcal{S}$ under the H_1 hypothesis. As in [11], [19], we propose to maximize over a subset of partitions $\mathcal{G}(\mathcal{S})$ of the scene under test. A possible choice for the elements of the set $\mathcal{G}(\mathcal{S})$ is given in Fig. 1: the dark zone represents the set $\mathcal{S}_1$, while the white one indicates the set $\mathcal{S}_0$; more details on such choice are given in Sect. III. The above derivation can be straightforwardly extended to the case that returns from more than one frequency band are available. To this end, we denote by $\boldsymbol{r}^{(B)}$ the polarimetric vector obtained by stacking up the vectors associated with returns from pixels of the region under test in the B frequency band, $\boldsymbol{r}_{i,j}^{(B)}$, $(i,j) \in \mathcal{S}$, say. The GLRT on two frequency bands can be re-written as

$$\min_{h\in\{0,1\}} \max_{\mathcal{P}_{\mathcal{S}}\in\mathcal{G}(\mathcal{S})} \Lambda^{(B_1)}(\boldsymbol{r}^{(B_1)})\Lambda^{(B_2)}(\boldsymbol{r}^{(B_2)}) \underset{H_0}{\overset{H_1}{\lessgtr}} \gamma \tag{5}$$

where

$$\Lambda^{(B)}(\boldsymbol{r}^{(B)}) = \frac{\widetilde{\Gamma}_N\left(\nu_h^{(B)}\right)}{\widetilde{\Gamma}_N\left(\nu_h^{(B)}+M\right)} \times \frac{\left|\sum_{(i,j)\in\mathcal{S}} \boldsymbol{r}_{i,j}^{(B)}\boldsymbol{r}_{i,j}^{(B)\dagger} + \left(\nu_h^{(B)}-N\right)\overline{\boldsymbol{M}}_h^{(B)}\right|^{\nu_h^{(B)}+M}}{\left|\left(\nu_h^{(B)}-N\right)\overline{\boldsymbol{M}}_h^{(B)}\right|^{\nu_h^{(B)}}} \times \frac{\widetilde{\Gamma}_N\left(\nu_0^{(B)}+M_0\right)}{\left|\sum_{(i,j)\in\mathcal{S}_0} \boldsymbol{r}_{i,j}^{(B)}\boldsymbol{r}_{i,j}^{(B)\dagger} + \left(\nu_0^{(B)}-N\right)\overline{\boldsymbol{M}}_0^{(B)}\right|^{\nu_0^{(B)}+M_0}} \times \frac{\widetilde{\Gamma}_N\left(\nu_1^{(B)}+M_1\right)}{\left|\sum_{(i,j)\in\mathcal{S}_1} \boldsymbol{r}_{i,j}^{(B)}\boldsymbol{r}_{i,j}^{(B)\dagger} + \left(\nu_1^{(B)}-N\right)\overline{\boldsymbol{M}}_1^{(B)}\right|^{\nu_1^{(B)}+M_1}}. \quad (6)$$

GLRTs (4) and (5) will be referred to in the following as Bayesian edge detectors (B-EDs).

III. Performance Assessment

In this section, we assess the performance of the proposed algorithm using both simulated and real data. For comparison purposes we also consider a previously proposed, classical (i.e., non-Bayesian) ED, referred to in the following as deterministic ED (D-ED) [8], [9], [11], [12]. All of the needed parameters have been set based on a polarimetric and multifrequency SAR image (L and C frequency bands) collected during the SIR-C/X-SAR mission. More specifically, we have processed non-calibrated, single-look complex data of the North Sea (Germany) collected at $54^o58'N$ $7^o45'E$, October 6, 1994, with resolution of 22 m in ground range and 6.2 m in azimuth. In particular, both EDs assume $N = 3$ and use VV, HH, and VH+HV polarimetric channels. An image of the sensed scene is displayed in Fig. 2: it contains several slicks, deployed as part of an experimental campaign aimed at assessing to what extent polarimetric and multifrequency SAR data could be exploited for detecting surface films with different viscoelastic properties, see [6], [12] and references therein for more details. Remember that the B-ED requires knowledge of the matrices $\overline{\boldsymbol{M}}_1^{(B)}$ and $\overline{\boldsymbol{M}}_0^{(B)}$. To this end, we have estimated $\overline{\boldsymbol{M}}_0^{(B)}$, $B = L, C$, by the sample covariance matrix based on the overall data of the available SIR-C/X-SAR image in the B band. As to $\overline{\boldsymbol{M}}_1^{(B)}$, we have used the following matrices $\overline{\boldsymbol{M}}_1^{(C)} = \sigma^{2(C)}\text{diag}(6,3,2)$ and $\overline{\boldsymbol{M}}_1^{(L)} = \sigma^{2(L)}\text{diag}(13,4,1)$ with $\sigma^{2(C)} = \sigma^{2(L)} = 10^{-3}$. Again, the values on the diagonal of the above matrices roughly fit those obtainable from real data (over pixels of the slicks). Moreover, the B-ED assumes $\nu_h^{(B)} = 5$, $h = 0, 1$, corresponding to a high variability of the $\boldsymbol{R}_{i,j}$s. The P_{fa} is set to 10^{-3} and the corresponding thresholds have been evaluated over 10^5 Monte Carlo runs using data simulated according to the models described in Section II with $h = 0$ (slick-free area). We have thus applied the B-ED and the D-ED to the simulated image of Fig. 3 and to the real image shown in Fig. 2. The tests have been applied over overlapping windows (of M pixels) with the current one obtained by shifting the previous window of 1 pixel in range or in azimuth. In Figs. 4-5 we report the output of the EDs, fed by the synthetic image of Fig. 3, for the case $M = 16$: the superiority of the B-ED, compared to the D-ED, is apparent, while for $M = 64$ (not reported here for brevity) the two EDs provide a similar performance. In Figs. 6-7 we report, instead, results obtained applying tests to the real data data corresponding to the scene depicted in Fig. 2. The original image has been decimated by a factor 2 in range and 3 in azimuth in order to come up with independent adjacent pixels [20] (given the VV or HH polarimetric channel, and given the $\boldsymbol{R}_{i,j}$). We set $M = 100$ in order to obtain satisfactory performance on real data ($M = 64$ provides practically the same performance). Inspection of the figures highlights that five out of the seven deployed slicks are detected. Summarizing, it is apparent that the B-ED guarantees an actual P_{fa} closer to the nominal one (i.e., 10^{-3}) than that of the D-ED; moreover, the detectors have almost the same power; actually, the B-ED is slightly superior to the D-ED. As a final comment, it is instructive to note that the B-EDs are not so different from their classical counterparts; however, in the proposed schemes, we have introduced the a priori knowledge, namely the $\overline{\boldsymbol{M}}_h^{(B)}$s, that counterbalances, in a way depending on the $\nu_h^{(B)}$s, the influence of the sample covariance matrices estimated on the data.

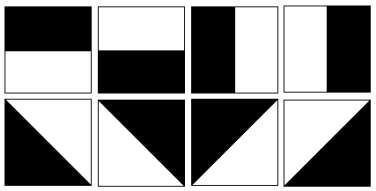

Fig. 1. Templates used to maximize the likelihood function under H_1: the black zone represents $\mathcal{S}_1$.

Fig. 2. SIR-C/X-SAR image under test (C-Band, VV polarization), 1000 pixels in range and 5000 in azimuth.

References

[1] H. A. Espedal, O. M. Johannessen, J. A. Johannessen, E. Dano, D. Lyzenga, J. Knulst, "COASTWATCH '95:ERS-1/2 Detection of Natural Film on the Ocean Surface," *J. Geophys. Res.*, Vol. 103, No. C11, pp. 24,969-24,982, Oct. 1998.

[2] F. Del Frate, A. Petrocchi, J. Lichtenegger, G. Calabresi, "Neural Networks for Oil Spill Detection Using ERS-SAR Data," *IEEE Trans. Geosci. Remote Sens.*, Vol. 38, No. 5, pp. 2282-2287, Sep. 2000.

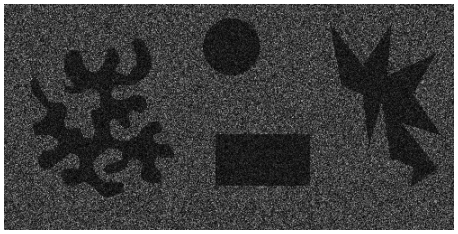

Fig. 3. A synthetic image generated using the models in Section II and according to the SAR image of the North Sea in the C frequency band (see the scene depicted in Fig. 2).

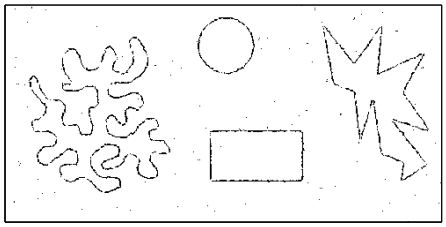

Fig. 4. Output of the B-ED with $M = 16$ fed by synthetic (single frequency and polarimetric) data corresponding to the scene depicted in Fig. 3.

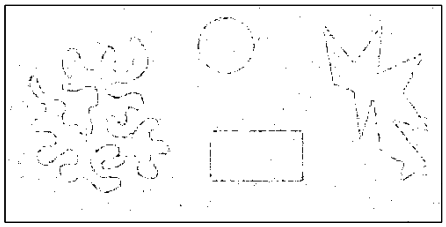

Fig. 5. Output of the D-ED with $M = 16$ fed by synthetic (single frequency and polarimetric) data corresponding to the scene depicted in Fig. 3.

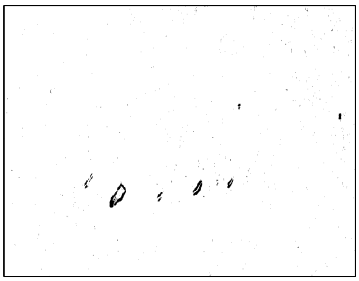

Fig. 6. Output of the B-ED fed by the SAR data of the North Sea in the C and L frequency bands with $M = 100$ (see the scene depicted in Fig. 2). Results are based on the nominal threshold to guarantee $P_{fa} = 10^{-3}$.

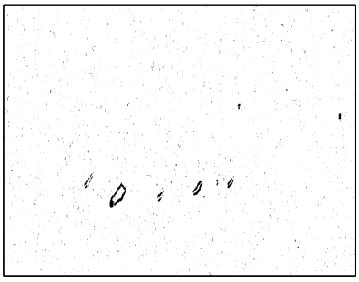

Fig. 7. Output of the D-ED fed by the SAR data of the North Sea in the C and L frequency bands with $M = 100$ (see the scene depicted in Fig. 2). Results are based on the nominal threshold to guarantee $P_{fa} = 10^{-3}$.

[3] B. Fiscella, A. Giancaspro, F. Nirchio, P. Pavese, P. Trivero, "Oil Spill detection using marine SAR images," *Int. J. Remote Sens.*, Vol. 18, pp. 3,561-3,566, Dec. 15, 2000.

[4] A. H. Schistad Soldberg, G. Storvik, R. Soldberg, E. Volden, "Automatic Detection of Oil Spills in ERS SAR Images," *IEEE Trans. Geosci. Remote Sens.*, Vol. 37, No. 4, pp. 1916-1924, Jul. 1999.

[5] A. Gambardella, A, Giacinto, M. Migliaccio, A. Montali, "One-class classification for oil spill detection," *Pattern Anal. Appl.*, Vol. 13, No. 3, pp. 349-366, Aug. 2010.

[6] M. Gade, W. Alpers, H. Huhnerfuss, H. Masuko, T. Kobayashi, "Imaging of biogenic and anthropogenic ocean surface films by the multifrequency/multipolarization SIR-C/X-SAR," *J. Geophys. Res.*, Vol. 103, No. C9, pp. 18,851-18,866, Aug. 15, 1998.

[7] P. Lombardo, D. I. Conte, A. Morelli, "Comparison of Optimised Processors for the Detection and Segmentation of Oil Slicks with Polarimetric SAR Images," *IGARSS2000*, Honolulu, Hawaii, USA, Jul. 24-28, 2000.

[8] K. Conradsen, A. A. Nielsen, J. Schou, H. Skriver, "A Test Statistic in the Complex Wishart Distribution and Its Application to Change Detection in Polarimetric SAR Data," *IEEE Trans. Geosci. Remote Sens.*, Vol. 41, No. 1, pp. 4-19, Jan. 2003.

[9] J. Schou, H. Skriver, K. Conradsen, A. A. Nielsen, "CFAR edge detector for polarimetric SAR images," *IEEE Trans. Geosci. Remote Sens.*, Vol. 41, No. 1, pp. 20-32, Jan. 2003.

[10] F. Bandiera, G. Ricci, M. Tesauro, "Trained and Non-Trained CFAR Detection of Oil Slicks on the Ocean Surface by Resorting to SAR Data," *7th International Symposium on Signal Processing and its Applications, ISSPA2003*, Paris, France, Jul. 1-4, 2003.

[11] F. Bandiera, G. Ricci, "Slicks Detection on the Sea Surface based upon Polarimetric SAR Data," *IEEE Geosci. Remote Sens. Lett.*, Vol. 2, No. 3, pp. 342-346, Jul. 2005.

[12] M. Migliaccio, A. Gambardella, M. Tranfaglia, "SAR Polarimetry to Observe Oil Spills," *IEEE Trans. Geosci. Remote Sens.*, Vol. 45, No. 2, pp. 506-511, Feb. 2007.

[13] M. Migliaccio, F. Nunziata, A. Montuori, C. Brown, "Marine added-value products by RADARSAT-2 fine quad-polarization," *Can. J. Remote Sens.*, Vol. 37, No. 5, pp. 443-451, Oct. 2011.

[14] M. Migliaccio, F. Nunziata, A. Montuori, Li Xiaofeng, W. G. Pichel, "A Multifrequency Polarimetric SAR Processing Chain to Observe Oil Fields in the Gulf of Mexico," *IEEE Trans. Geosci. Remote Sens.*, Vol. 49, No. 12, pp. 4729-4737, Dec. 2011.

[15] F. Bandiera, O. Besson, G. Ricci, "Knowledge-Aided Covariance Matrix Estimation and Adaptive Detection in Compound-Gaussian Noise," *IEEE Trans. Signal Process.*, Vol. 58, No. 10, pp. 5390-5396, Oct. 2010.

[16] F. Bandiera, O. Besson, G. Ricci, "Adaptive detection of distributed targets in compound-Gaussian noise without secondary data: a Bayesian approach," *IEEE Trans. Signal Process.*, Vol. 59, No. 12, pp. 5698-5708, Dec. 2011.

[17] T. W. Anderson, *An Introduction to Multivariate Statistical Analysis*, 3rd ed., John Wiley & Sons, 2003.

[18] A. Gelman, J. B. Carlin, H. S. Stern, D. B. Rubin, *Bayesian Data Analysis, 2nd ed.*, New York: Chapman & Hall, 2004.

[19] R. Touzi, A. Lopes, P. Bousquet, "A Statistical and Geometrical Edge Detector for SAR Images," *IEEE Trans. Geosci. Remote Sens.*, Vol. 26, No. 6, pp. 764-773, Nov. 1988.

[20] A. Fusco, C. Galdi, G. Ricci, M. Tesauro, "Fitting a Statistical Model to SIR-C SAR Images of the Sea Surface," *IEEE Trans. Aerosp. Electron. Syst.*, Vol. 40, No. 4, pp. 1179-1190, Oct. 2004.